ChemComm

COMMUNICATION

View Article Online
View Journal | View Issue

Cite this: *Chem. Commun.*, 2014, **50**, 10510

Received 29th May 2014,
Accepted 22nd July 2014

DOI: 10.1039/c4cc04124k

www.rsc.org/chemcomm

Pd nanoparticle concentration dependent self-assembly of Pd@SiO_2 nanoparticles into leaching resistant microcubes†

Abheek Datta,[a] Anustup Sadhu,[a] Subhankar Santra,[a] S. M. Shivaprasad,[b] Swadhin K. Mandal[a] and Sayan Bhattacharyya*[a]

Pd NP concentration guided the self-assembly of core–shell Pd@SiO_2 nanoparticles (NPs) into microcubes. The Pd NPs were stacked by molten dodecyltrimethylammonium bromide (DTAB) to create the SiO_2 envelope. The microcubes demonstrated improved leaching resistance in heterogeneous catalysis over a conventional porous support.

Although discrete NPs could be easily synthesized by surfactant assisted wet-chemical routes, easy handling of these NPs requires well-defined superstructures for practical applications.[1,2] In the past, the self-assembled superstructures or microstructures were obtained by solvent evaporation,[3] surfactant templates,[4,5] or molecular cross-linking.[6] Molecular simulations have shown that NPs coated with surfactants can self-assemble into larger structures based on solvent selectivity of the NPs and the surfactants.[7] NPs tend to remain aggregated in order to minimize their free energy and the self-assembled shapes are dependent on a particular solvent medium. The self-assembly processes have been so far shown to be dependent on specific and non-specific interactions of the surfactants with the NPs. Also, the shape and size of nanocomposites are known to be engineered by the NPs and surfactants.[8–11] However, keeping the synthesis parameters constant, the self-assembly process was never observed to be guided by the NP concentration.

In most of the metal NP and SiO_2 composites, the shape of the SiO_2 support was governed by the organic linkers and the metal NPs were added post-fabrication of the support.[12,13] Quite a few studies are available on *in situ* synthesis where the metal NPs occupy site selective locations.[14–16] The Pd NP–SiO_2 composites are excellent heterogeneous catalysts in the formation of C–C and C–X (X = Cl, Br, I) bonds.[12,17,18] Self-assembly of an ensemble of Pd NPs into 3-dimensional (3D) micron-sized architectures can improve the robustness of the system, still maintaining the novel properties of the NPs. A precise knowledge of the metal NP distribution is necessary such as if the NPs are immobilized on the outer surface or embedded inside the support to understand the transport of reactant molecules to the active sites.[18,19] The designed 3D composites should offer improved control over the surface chemistry and NP size, which are key factors in the construction of next generation catalysts.

Herein we demonstrate the morphology evolution of porous silica to non-porous Pd–SiO_2 microcubes aided by <0.5 wt% Pd NPs and DTAB. Acid hydrolysis of TEOS in the presence of DTAB generated porous SiO_2 and with the optimal presence of Pd NPs in the solution, micron sized cubes of SiO_2 was formed. Acid hydrolysis was carried out with different concentrations of Pd NPs separately in air and N_2 to synthesize the as-synthesized (AS) products which were hydrogenated at 550 °C. ICP-MS analyses of the hydrogenated (H-550) Pd–SiO_2 composites provided the final weight% of Pd NPs. Two Pd–SiO_2 composites were synthesized in N_2 with Pd wt% of 0.09 and 0.34, whereas those synthesized in air had Pd wt% of 0.14 and 0.41. Also a separate sample was synthesized where 0.37 wt% Pd NPs were exclusively immobilized on the surface of mesoporous SiO_2 by a PVP binder. Fig. 1a shows the transmission electron micrograph (TEM) of the pristine citrate ligand stabilized spherical Pd NPs of diameter 4.3 ± 0.4 nm. The inter-planar spacing of 0.23 nm corresponds to the (111) reflection. The X-ray diffraction (XRD) patterns of the H-550 composites correspond to metallic Pd^0 (JCPDS No. 87-0639) over a background of amorphous SiO_2 (Fig. S2, ESI†).

The morphological trends are similar in the AS (Fig. S3, ESI†) and H-550 composites (Fig. 1 and Fig. S4, ESI†). In the absence of Pd NPs, porous SiO_2 was obtained. With <0.2 wt% Pd NPs, 10–20 nm well-defined spherical clusters were formed, and these particles aggregated into $\sim$600 nm diameter spheres (Fig. 1b). The clusters consisted of SiO_2 shell encapsulated Pd NPs. When 0.34–0.41 wt% Pd NPs were present, grooved SiO_2 microcubes were observed (Fig. 1d and g). In fact, a threshold of

[a] *Department of Chemical Sciences, Indian Institute of Science Education and Research (IISER) Kolkata, Mohanpur – 741246, India. E-mail: sayanb@iiserkol.ac.in*
[b] *International Centre for Materials Science & Chemistry and Physics of Materials Unit, Jawaharlal Nehru Centre for Advanced Scientific Research, Jakkur, Bangalore – 560064, India*

† Electronic supplementary information (ESI) available: Experimental section, XRD patterns, FESEM images, details of surface area, ^{1}H NMR, FTIR and XPS measurements, control experiments and catalysis standardization. See DOI: 10.1039/c4cc04124k

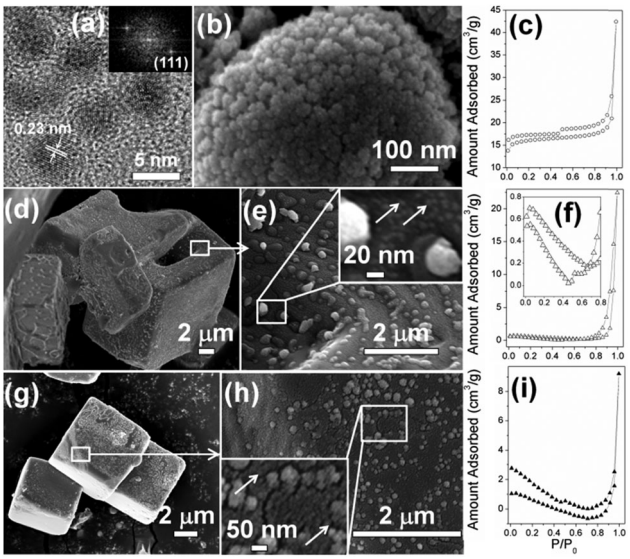

Fig. 1 (a) High-resolution TEM image of pristine Pd NPs and (inset) FFT pattern. FESEM images of H-550 Pd–SiO_2 composites with Pd wt% of (b) 0.14 (air), (d) 0.41 (air), (e) enlarged view of the marked area in (d), (g) 0.34 (N_2) and (h) enlarged view of the marked area in (g). Arrows inside the insets show Pd NPs. N_2 adsorption–desorption isotherms with Pd wt% of (c) 0.14, (f) 0.41 and (i) 0.34. Inset (f) shows the low pressure hysteresis.

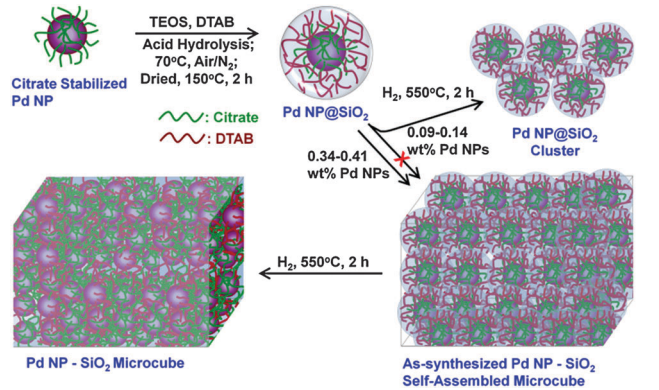

Fig. 2 Schematic illustration of the formation process of Pd–SiO_2 microcubes.

~0.2 wt% Pd NPs was required to form the microcubes. An enlarged view of the field emission scanning electron microscopy (FESEM) images in Fig. 1e and h shows that there are 100–200 nm clusters and Pd NPs dispersed both inside and outside the microcubes. The inhomogeneous distribution of Pd NPs was examined by energy dispersive analysis of X-ray (EDAX) spectra (Fig. S5, ESI†) and the concentration of Pd was higher inside the grooves of the microcubes than on the surface. With ~1 wt% Pd NPs, almost all the Pd NPs remain confined inside the microcubes with fewer grooves (Fig. S6, ESI†).

Pd NPs converted the porous SiO_2 into non-porous Pd–SiO_2 microcubes as evident from the N_2 adsorption–desorption isotherms in Fig. 1, Fig. S7 and S8 (ESI†). In the absence of Pd NPs, SiO_2 had a decent surface area of 574–581 $m^2\ g^{-1}$ with type IV physisorption isotherm and H2 hysteresis loop, indicative of mesopores (Fig. S9, ESI†).[20] When the AS samples were hydrogenated, two competing factors of shrinkage of pores and decomposition of surfactants determine the change in surface area. With the addition of <0.2 wt% Pd, the surface area of the AS samples dropped to 8–11 $m^2\ g^{-1}$, primarily due to partial collapse of the mesoporous matrix and formation of Pd@SiO_2 core–shell particles. The physisorption isotherms of the AS and H-550 0.09–0.14 wt% Pd@SiO_2 samples did not possess limiting adsorption at high relative pressure (H3 type hysteresis loop). The physisorption isotherms of the ≥0.2 wt% Pd samples possessed H3 type hysteresis with minimum surface area and negligible micropores (Fig. 1f and i). After hydrogenation, decomposition of the surfactants did not lead to new pores. Significant low pressure hysteresis was observed, which is associated with the irreversible uptake of adsorbate (N_2) molecules within Å-wide diameter pores. Bond formation and breaking of the citrate and DTAB molecules could result in pore dimensions comparable to the diameter of the N_2 molecules. Once adsorbed into the Å-wide pores, the adsorbate molecules could not be desorbed.

The SiO_2 microcubes were formed with Pd NPs situated both inside and outside the cubes (Fig. 2). The Pd NPs were stabilized by electrostatic repulsion due to the presence of citrate ions adsorbed on their surface. When DTAB $[CH_3(CH_2)_{11}N^+(CH_3)_3Br^-]$ was added to the Pd NPs in the presence of TEOS at acidic pH, DTAB could bind to the negatively charged citrate groups and the hydrolysis of TEOS took place around the ~4.3 nm Pd NPs to form core–shell Pd–SiO_2 particles of diameter 10–20 nm. The self-assembly of these core–shell particles was strongly intertwined with the concentration of Pd NPs and DTAB. The AS products were dried at 150 °C, and DTAB with a melting point of 246 °C could not decompose completely even in air. Secondly the formation of cubes required layer-by-layer stacking of a threshold ~0.2 wt% Pd NP support and below this critical loading, the cubes were not obtained. In the AS samples with ≥0.2 wt% Pd NPs, complete stacking could take place at 150 °C due to partial decomposition of DTAB. The SiO_2 envelope remained discontinuous and the microcubes were deformed and grooved. During hydrogenation, DTAB remains in the molten state at 550 °C but still could not decompose completely due to the absence of atmospheric oxygen. The molten DTAB breaks the SiO_2 shell over the Pd@SiO_2 NPs and the core–shell morphology disintegrates, which helps silica to form a continuous envelope around the Pd NPs upon cooling. DTAB acts as the carrier of silica over an ensemble of stacked Pd NPs. Thermogravimetric analysis has shown that ~14 wt% DTAB contributed in the morphological transformation and 6–10 wt% DTAB helped in stabilizing the microcubes (Fig. S10, ESI†). However, the assembly of the Pd NPs inside the cubes is guided by the stacking process in the AS precursor. Thus several deformations and grooves were observed in the H-550 cubes. Due to this non-uniformity in stacking, Pd@SiO_2 NPs were observed even on the surface of the microcubes. Generally, in cubic NPs a large fraction of atoms reside on the edges and vertices which leads to high free energy.[21] The microcubes could be stabilized since with increase in size, the contribution from the edges and vertices to the overall free energy decreases.

FTIR spectra showed that a lesser concentration of DTAB was still retained in the H-550 samples (Fig. S11, ESI†). An optimum

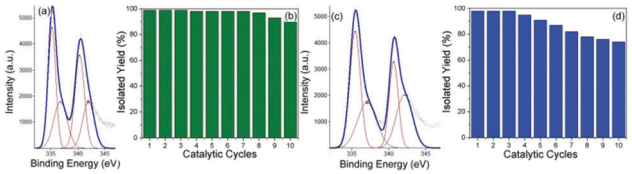

Fig. 3 (a, c) Pd 3d XPS spectra and (b, d) isolated yield of the product after recycling the catalysts for up to 10 cycles for 0.41 wt% P–SiO_2 microcubes (a, b) and 0.37 wt% Pd NP–porous SiO_2 (c, d), respectively.

of 0.05 g DTAB is crucial in stabilizing the microcubes, without which well-defined cubes shapes were not obtained (Fig. S12, ESI†). In fact, anionic and neutral surfactants also gave irregular cube-like shapes. This emphasizes that irrespective of an electrostatic interaction to bind Pd NPs to SiO_2, the stacking of Pd NPs will take place depending on the Pd NP concentration in the presence of a surfactant.

Although, TEM and XRD did not provide any evidence of Pd^{2+} species, X-ray photoelectron spectroscopy (XPS) analyses showed the presence of 36–37% and 43–49% amorphous PdO in H-550 0.41 wt% Pd–SiO_2 (air) and 0.37 wt% Pd deposited outside mesoporous SiO_2, respectively (Fig. 3). The extent of oxidation is less when part of the Pd NPs is confined inside the SiO_2 microcubes. In the microcubes, the Si–OH species was also observed along with SiO_2, where the peaks at 103.6 and 103.9 eV are due to Si–OH bonds in SiO_2 and hydroxylated SiO_2, respectively (Fig. S13, ESI†).[22]

To study the dependence of the yield and recyclability in Suzuki–Miyaura C–C cross coupling on the catalyst morphology, the performance of H-550 0.41 wt% Pd–SiO_2 microcubes was compared to the 0.37 wt% Pd NPs immobilized on mesoporous SiO_2. In the coupling of phenylboronic acid and 4-bromotoluene an optimum activity was obtained when K_2CO_3 was the base and DMF : H_2O (1 : 3) the solvent (Table S15, ESI†). The initial turnover numbers were 5183 and 5799 for the microcubes and mesoporous catalysts with Pd wt% of 0.41 and 0.37, respectively (Fig. S16, ESI†). Fig. 3 shows the recyclability performance of the catalysts in 10 runs. Although the initial yields were similar, the mesoporous catalyst was deactivated from the 4th catalytic cycle. The microcubes retain decent catalytic activity throughout. The microcubes showed excellent leaching resistance since majority of the Pd NPs was embedded inside the cube. The slight drop in yield% from the 8th cycle was due to leaching of the unprotected Pd NPs from the microcube surface. In contrast, when all the Pd NPs remain attached to the surface of mesoporous SiO_2, the chance of leaching of the NPs is higher. However, the microcubes were non-porous (Fig. 1c, f and i) and the reactant molecules could enter through the Å-sized pores but the Pd NPs could not leach out. It was also observed by FESEM studies that after the 5th and 10th cycle, the microcubes retain their bulk morphology but the mesoporous structure was ruptured (Fig. S17, ESI†). The strong network of Pd@SiO_2 NP stacks and surfactant scaffold holds the cubic microstructure and generates NP leaching resistance.

In summary, morphology evolution of SiO_2 aided by ~4.3 nm Pd NPs was demonstrated whereby ~0.1 wt% Pd NPs could transform porous SiO_2 into 10–20 nm Pd@SiO_2 NPs. Self-assembly of ≥0.2 wt% Pd@SiO_2 NPs resulted in Pd–SiO_2 non-porous microcubes. Incomplete decomposition of the surfactant DTAB under H_2 at 550 °C helps SiO_2 to form a continuous envelope around the stacked ensemble of Pd NPs which self-assemble to form grooved microcubes upon cooling. The Pd–SiO_2 microcubes demonstrated superior leaching resistance. The Pd NP governed self-assembly process can be extended to other NPs for creating self-assembled microstructures for a wide range of practical applications in catalysis, bio-reactors, molecular separation media, and optical and magnetic devices.

This work is supported by Department of Science and Technology (DST), Government of India, under grant no. SR/S1/PC-28/2011. AD thanks University Grants Commission (UGC), New Delhi, for his fellowship.

Notes and references

1 M. Li, H. Schnablegger and S. Mann, *Nature*, 1999, **402**, 393–395.
2 Y. Deng, Y. Cai, Z. Sun, J. Liu, C. Liu, J. Wei, W. Li, C. Liu, Y. Wang and D. Jhao, *J. Am. Chem. Soc.*, 2010, **132**, 8466–8473.
3 G. V. R. Rao, G. P. López, J. Bravo, H. Pham, A. K. Datye, H. Xu and T. L. Ward, *Adv. Mater.*, 2002, **14**, 1301–1304.
4 Th. Zemb, M. Dubois, B. Demé and Th. Gulik-Krzywicki, *Science*, 1999, **283**, 816–819.
5 X. Ji, Q. Hu, J. E. Hampsey, X. Qiu, L. Gao, J. He and Y. Lu, *Chem. Mater.*, 2006, **18**, 2265–2274.
6 K. L. Hamner, C. M. Alexander, K. Coopersmith, D. Reishofer, C. Provenza and M. M. Maye, *ACS Nano*, 2013, **7**, 7011–7020.
7 Z. Zhang, M. A. Horsch, M. H. Lamm and S. C. Glotzer, *Nano Lett.*, 2002, **14**, 1301–1304.
8 D. A. Walker, E. K. Leitsch, R. J. Nap, I. Szleifer and I. Grzybowski, *Nat. Nanotechnol.*, 2013, **8**, 676–681.
9 G. Liu, K. L. Young, X. Liao, M. L. Personick and C. A. Mirkin, *J. Am. Chem. Soc.*, 2013, **135**, 12196–12199.
10 S. Bhattacharyya and A. Gedanken, *J. Phys. Chem. C*, 2008, **112**, 659–665.
11 S. Bhattacharyya and A. Gedanken, *J. Phys. Chem. C*, 2008, **112**, 13156–13162.
12 G. Park, S. Lee, S. Son and S. Shin, *Green Chem.*, 2013, **15**, 3468–3473.
13 P. Li, H. Liu, Y. Yu, C.-Y. Cao and W.-G. Song, *Chem. – Asian J.*, 2013, **8**, 2459–2465.
14 L. Li, D. L. King, J. Liu, Q. Huo, K. Zhu, C. Wang, M. Gerber, D. Stevens and Y. Wang, *Chem. Mater.*, 2009, **21**, 5358–5364.
15 H. Song, R. M. Rioux, J. D. Hoefelmeyer, R. Komor, K. Niesz, M. Grass, P. Yang and G. A. Somorjai, *J. Am. Chem. Soc.*, 2006, **128**, 3027–3037.
16 L. Chen, J. Hu, Z. Qi, Y. Fang and R. Richards, *Ind. Eng. Chem. Res.*, 2011, **50**, 13642–13649.
17 Z. Chen, Z. M. Cui, F. Niu, L. Jiang and W. G. Song, *Chem. Commun.*, 2010, **46**, 6524–6526.
18 J. C. Park, E. Heo, A. Kim, M. Kim, K. H. Park and H. Song, *J. Phys. Chem. C*, 2011, **115**, 15772–15777.
19 S. M. Kim, M. Jeon, K. W. Kim, J. Park and I. S. Lee, *J. Am. Chem. Soc.*, 2013, **135**, 15714–15717.
20 K. S. W. Sing, D. H. Everett, R. A. W. Haul, L. Moscou, R. A. Pierrotti, J. Rouquerol and T. Siemieniewska, *Pure Appl. Chem.*, 1985, **57**, 603–619.
21 A. S. Barnard and P. A. Zapol, *J. Chem. Phys.*, 2004, **121**, 4276–4283.
22 M. L. Miller and R. W. Linton, *Anal. Chem.*, 1985, **57**, 2314–2319.

